Cellulose
https://doi.org/10.1007/s10570-023-05162-3

ORIGINAL RESEARCH

Isolation of cellulose microfibers and nanofibers by mechanical fibrillation in a water-free solvent

E. Hernández-Becerra · M. Osorio · D. Marín · P. Gañán · M. Pereira · D. Builes · C. Castro

Received: 19 May 2022 / Accepted: 18 March 2023

Abstract Cellulose from vegetable sources is the most abundant biopolymer on earth. In plants, cellulose is a reinforcement element that conforms to a hierarchical structure. Cellulose micro-/nanofibers can be isolated from the cell wall by top-down strategies involving mechanical processes to be used in applications as a reinforcing material. Nonetheless, its use has been limited as its extraction in an aqueous medium is unfavorable when employed in low-hydrophilic matrices. Therefore, this work proposes a novel homogenization route in which cellulose micro-/nanofibers are directly obtained and dispersed in propylene glycol (PG), which generates more possibilities for these (nano) structures in applications that require water-free environments. Moreover, the influence on the cycle numbers in the morphological, chemical, thermal, and rheological properties was researched. Thus, the obtained micro-/nanofibers presented TEM diameters even below 20 nm. XRD analysis evidenced crystalline planes located at $1\bar{1}0$, 110, and 200, and crystallinity degree values up to 80%. Also, FTIR spectra bands in 3340 cm^{-1}, 2890 cm^{-1}, 1314 cm^{-1}, and in the fingerprint region corresponded to native cellulose Iβ. FTIR and TGA confirmed no influence of mechanical cycles on cellulose fibers' chemical and thermal properties. Furthermore, the increase in the cycle number evidenced a shear-thinning rheological behavior of the suspensions. Considering the above results, it was concluded that the proposed high-pressure homogenization within PG is an approach for vegetable nanocellulose homogenization while maintaining high crystallinity, thermal, and chemical features with huge importance for subsequent processes in the development of nanocomposites with hydrophilic matrices for industrial applications.

Supplementary Information The online version contains supplementary material available at https://doi.org/10.1007/s10570-023-05162-3.

E. Hernández-Becerra · M. Osorio · P. Gañán · C. Castro (✉)
Engineering School, Universidad Pontificia Bolivariana, Circular 1 No. 70-01, Medellín, Colombia
e-mail: cristina.castro@upb.edu.co

M. Osorio · D. Marín
System Biology Research Group, School of Health Sciences, School of Medicine, Universidad Pontificia Bolivariana, Circular 1 No. 70-01, Medellín, Colombia

D. Marín · D. Builes
Research and Development Department, Andercol-Akzonobel, Calle 19A No. 43B-41, Medellín, Colombia

M. Pereira
Chemical Engineering Department, Universidad de Concepción, Concepción, Chile

Published online: 18 April 2023

Graphical abstract

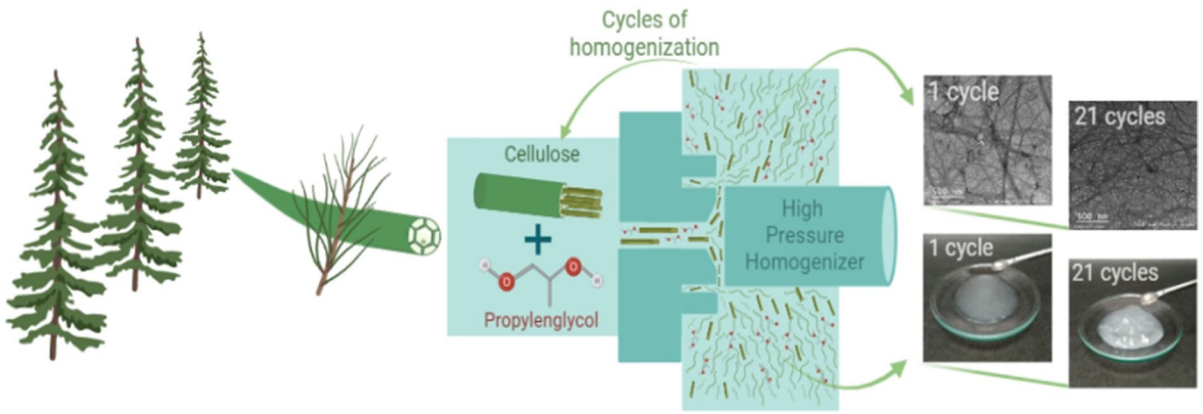

Keywords Vegetal cellulose · Water-free fibrillation · Propylene glycol · Micro-/nanofibers · Mechanical treatment

Introduction

Cellulose is the major biopolymer on Earth (Li et al. 2021). It is biosynthesized by plants, animals, and microorganisms (Moon et al. 2011) with an estimated annual synthesis by nature of ca. 10^{11}–10^{12} tons (Klemm et al. 1998). Due to their origin, plants are the most available source (Prakash Menon et al. 2017), building the cell walls with hemicellulose and lignin (Carpita and Gibeaut 1993). The hemicellulose has a structural role acting as reinforcement, while lignin acts as a matrix to aggregate the cellulose fibers (Ansell 2015). Thus, these cellulose fibrils are conformed by a hierarchical structure ranging from the nanoscale to macroscopic dimensions (Moon et al. 2011). They have a molecular structure composed of D-glucopyranosyl units linked by β-1,4 glycosidic bonds forming a linear chain (French 2017). The adjacent chains interact through hydrogen bonds, creating protofibrils, which aggregate in nanofibers (Moon et al. 2011). These nanofibers are assembled with hemicellulose and lignin, forming the natural structure of plant fibers (Ansell 2015).

The above-mentioned structural hierarchy can be disrupted with the implementation of top-down strategies involving mechanical and chemical processes to obtain cellulose microfibers (CMFs) and cellulose nanofibers (CNFs) (Dufresne 2019). The CNFs exhibit properties such as high specific surface area, low density, low cost, high specific strength, biodegradability, non-toxicity, and organic nature (Dufresne 2008; Oksman et al. 2016), optical performance, and barrier properties that give them many industrial applications in the paper industry (Małachowska et al. 2020), biomedical field (Seddiqi et al. 2021), engineered materials (Guan et al. 2021), among others (Barhoum et al. 2019; Trache et al. 2020; Mateo et al. 2021). Nevertheless, the use of polymeric nanocomposites is the major application of CNFs (Mondal 2018; Sharma et al. 2019; Omran et al. 2021; Bangar and Whiteside 2021; Amara et al. 2021).

The CNFs have been used in composites-type materials as a reinforcement biopolymer. For instance, cellulose has been used to reinforce polymeric material due to its advantageous physicochemical features, versatility, and renewability (Shaghaleh et al. 2018). However, its use is limited due to its hydrophilic functional groups (hydroxyl groups) and the hydrophobic characteristics of most of the polymers (Medronho et al. 2012), which cause difficulties in achieving acceptable dispersion levels and generation of agglomerates during processing, thus leading to ineffective composites (Chanda and Bajwa 2021). Moreover, the CNF extraction is usually

accomplished in an aqueous medium which is also unfavorable for organic and highly hydrophobic polymeric synthetic matrices (Builes et al. 2013).

To improve its dispersion in a composite performance, authors including Ferreira et al. (2018) have suggested some methods, such as the chemical surface modification based on the substitution of hydrophilic OH groups on cellulose surface by more hydrophobic groups compatible with hydrophobic matrices (Ferreira et al. 2018). Nevertheless, functionalization processes may involve time-consuming synthesis, toxic reagents, and critical control of the reactions (Chanda and Bajwa 2021).

Another alternative is the employment of coupling or dispersing agents (Poletto and Zattera 2017) and the use of solvent exchange methods (Andrade et al. 2021). Several studies reported the use of solvent exchange to improve the dispersibility of nanocellulose in a polymer matrix. CNFs have been successfully dispersed in organic solvents, such as ethanol (Kaldéus et al. 2018), dimethylsulfoxide (DMSO) (Jiang et al. 2019), *N*,*N*-dimethylformamide (DMF) (Phadagi et al. 2021), ethylene glycol (EG) and propylene glycol (PG) (Wang et al. 2019). Wang et al. (2019) developed a methodology in which CNFs were obtained by a top-down process from a water suspension of cellulose pulp using mechanical stress. However, the authors employed a solvent-exchange method where CNFs were passed through different incremental water:water-free solvent mixing with glycols until reaching the pure solvent suspension (Wang et al. 2019). Nonetheless, the above strategies are time-consuming, energetically demanding, and chemically expensive (Wang et al. 2021).

Therefore, this study proposes a new methodology to incorporate and homogenize CNFs directly into an organic solvent, such as propylene glycol (PG), avoiding the high time consumption of solvent exchange methods and the solvent amount, and probably decreasing the cost of the process. The cellulose pulp was dispersed using a high-pressure homogenizer, including PG as the dispersion medium. The PG has a lower dielectric point compared to water and formed a dispersion containing the cellulose fibers, which was subjected to seven different cycles (from 1 to 21 cycles). The PG-Cellulose dispersion led to the obtention of micro-/nanofibrils with potential applications as reinforced materials in a low hydrophilic polymer matrix.

Experimental section

Materials

The raw materials corresponded to commercial bleached Kraft pulp sheets from *E. Globulus* (100% *E. Globulus*), provided by the company CMPC pulp S.A. in its Santa Fe Mill and Pacífico Mill, Chile. The chemical composition of the fiber corresponded to cellulose ($78.0 \pm 0.8\%$), hemicellulose xylanases (20.6 ± 0.3), and lignin ($< 1.0\%$).

Propylene glycol (PG, Mw 76.09 g/mol) was purchased from Sigma Aldrich.

Development of CMF and CNF dispersion in PG

In this study, bleached Kraft vegetal cellulose pulp was obtained from compact paper rolls, ripped into 1 cm^2 square. These paper portions were subjected to grinding in an IKA A11 mill for 1 min. Later, 10 wt% PG suspension was prepared and mixed for 4 h with a mechanical stirrer to reach the moistening. After this period, the suspension was passed through a PFI refiner until reaching 50,000 cycles. The suspension was diluted to 1 wt%, adding more PG, and homogenized for a few minutes with a mechanical stirrer. Finally, the mixture was subjected to 1, 3, 6, 12, 15, 18, and 21 cycles in a high-pressure homogenizer GEA with 800 bars of pressure.

Characterization techniques

Atomic force microscopy (AFM)

AFM was used to analyze micrometer-scale fibers or cellulose microfibers (CMFs). 100 µl of each sample was placed on a clean glass sample holder, dried at 60 °C overnight, and put in a desiccator to maintain low moisture. Then, the morphology of microfibers was analyzed using AFM with a scanning probe microscopy (Flex-Bio-Nano Surf), employing an ACL-A cantilever on the non-contact mode, PID: P: 1000, I: 3200, D: 0 with a free frequency of 50% and vibrational amplitude of 3 V.

The Gwyddion software was employed for the visualization, color, and contrast adjustment of AFM micrographs. For this, a mean plane subtraction was performed, followed by a making facet point upward.

Then, rows were aligned using various methods, the polynomial background was removed, and a shift to zero of the minimum data value was applied, followed by the local contrast adjustment. Finally, fiber length was measured by *ImageJ*, and the data were processed with *R Studio* software.

Transmission electron microscopy (TEM)

TEM was used to analyze nanometer-scale fibers or cellulose nanofibers (CNFs), providing real-space images of the system in the dried state, where local aggregates and fiber dimensions could be identified (Ogawa and Putaux 2019). 8 µL of the sample were deposited on a carbon gold mesh, dried at 60 °C, and stained with uranyl acetate (2 wt%) as a negative contrast agent. The samples were observed under a FEI Tecnai G2 F20 microscope at 80 kV. The fiber diameter was measured using *ImageJ*. The measurements were statically analyzed, as explained below for the AFM analysis.

X-ray diffraction (XRD)

X-ray crystallography was used to evaluate the crystallinity of the samples during mechanical fibrillation in PG. Dried films of cellulose fibers for the different cycles mentioned above were X-rayed using an Xpert PANalytical Empyrean II-Alpha1 diffractometer operating at a $K\alpha_1/K\alpha_2$ ratio of 0.5 with a radiation wavelength of 1.542 Å. Data were collected in reflection mode in the 5°–60° range with a step of 0.026°. The scans proceeded at 51.765 s per step. The diffraction peaks were fitted using Gaussian functions.

The d-spacings between the crystal planes were determined using Bragg's law.

$$D = \lambda/2\sin\theta \tag{1}$$

where θ is the angle between the plane and the diffracted or incident beam and λ is the wavelength of the X-rays. The apparent crystal size (ACS) was calculated using Scherrer's formula (Scherrer 1912).

$$ACS = 0.94\lambda/FWHM\cos\theta \tag{2}$$

where FWHM is the width of the peak at half the maximum height. θ is Bragg's angle, and λ is the wavelength of the X-rays.

The crystalline index (CrI) percentage was calculated according to Segal et al. (1959), including the intensity of the amorphous zone and crystalline peaks.

$$CrI\ (\%) = \left(I_{200} - I_{AM}/I_{200}\right) \times 100 \tag{3}$$

In this expression, the CrI expresses the degree of crystallinity, where I_{200} is the maximum intensity of the 200-lattice diffraction and I_{AM} is Segal's indicator for the amorphous contribution, taken as the minimum intensity between the (110) and (200) peaks at about 18.6° (Segal et al. 1959; French and Santiago Cintrón 2013; French 2020).

Fourier transform infrared spectroscopy (FTIR)

Infrared spectroscopy experiments were performed using an FTIR spectrometer (Nicolet 6700 Series) equipped with a single-reflection ATR and a type IIA diamond crystal mounted in tungsten carbide. Samples were dried at 60–70 °C for 7 days to reach the constant weight. The diamond ATR had a sampling area of approximately 0.5 mm^2, where a consistent reproducible pressure was applied to every sample. The infrared spectra were collected at 4 cm^{-1} resolutions over 128 scans in the 4000–400 cm^{-1} range.

Thermogravimetric analysis (TGA)

Samples were dried at 60–70 °C for 7 days to reach the constant weight followed by 1 h at 120 °C prior TGA measurements. Then, 12 mg were weighed and placed under a nitrogen atmosphere of 30 mL min^{-1} in a thermogravimetric analyzer (Mettler Toledo TGA/SDTA 851E) from 30 to 800 °C employing a heating rate of 10 °C min^{-1}.

Rheological analysis

Shear sweeps were carried out from 1 to 1000 s^{-1} in a hybrid rheometer Discovery HR-1 of TA Instruments, equipped with temperature control by a Peltier system under the lower plate. Samples dispersion (2.5 wt% of cellulose content) was measured at 25 °C, with a 40 mm diameter parallel plate and sample gap of 500 µm.

Statistical analysis

The statistical analysis was performed using the Kruskal–Wallis test as a non-parametric test, which makes it suitable for the fiber size distributions in this study (Ang et al. 2020). The statistical analysis and graphical processing were executed through *R Studio* software and *Origin* software. *P*-values < 0.05 were considered statistically significant.

For AFM analysis, 400 fiber diameters from every cycle (1 to 21) were measured across the image. Then, a mean diameter between every two measures was obtained, and the histogram distribution by size ranges was generated. The boxplots presented were built with the 400 measurements for each cycle but eliminating the outliers with *R Studio* software.

The diameter or width determination for TEM analysis was carried out through 60 measurements of the fibers in the TEM micrographs, which were subsequently processed. The outliers were also eliminated with *R Studio* software.

Results and discussion

Morphological analysis

The physical defibrillation processes of cellulose structures isolate micro-/nanofibers (Qasim et al. 2021). These processes lead to the formation of different fiber sizes, including micrometer and nanometer scale fibers. In Fig. 1, AFM micrographs show the fiber morphology after different homogenization cycles using PG during cellulose defibrillation. All samples showed top-down fiber morphology performing a random distribution of CMFs, which could be visualized either by individual fibers or packed bundles of CNFs. The bundles are kept together by hydrogen bonds (Osong et al. 2016).

The control sample presented a width or diameter c.a. 18.3 ± 0.4 µm (Andrade 2022). The homogenized mean fiber diameter of CMFs by AFM technique ranged from 146 to 364 nm. Thicker fibers were measured in all numbers of fibrillation cycles, probably because some fibers were not sufficiently fibrillated and kept their size through the high density of hydrogen bonds (Lee et al. 2009; Souza et al. 2019). The heterogeneity of the sizes is an expected phenomenon during vegetal cellulose physical fibrillation (Desmaisons et al. 2017).

Figures 2A, B evidence the heterogeneous size distribution of CMFs and CNFs, which correspond to the AFM images shown in Fig. 1. The histogram shows the percentual distribution of the fiber's diameter. From the 7 treatments, the measures corresponding to 12 cycles presented a higher broad distribution in histogram and boxplot compared to the other cycles. In Fig. 2A, all samples showed a positively skewed data distribution that does not follow a normal behavior (non-parametric Kruskal–Wallis test, *P*-value $< 2.2e{-}16$).

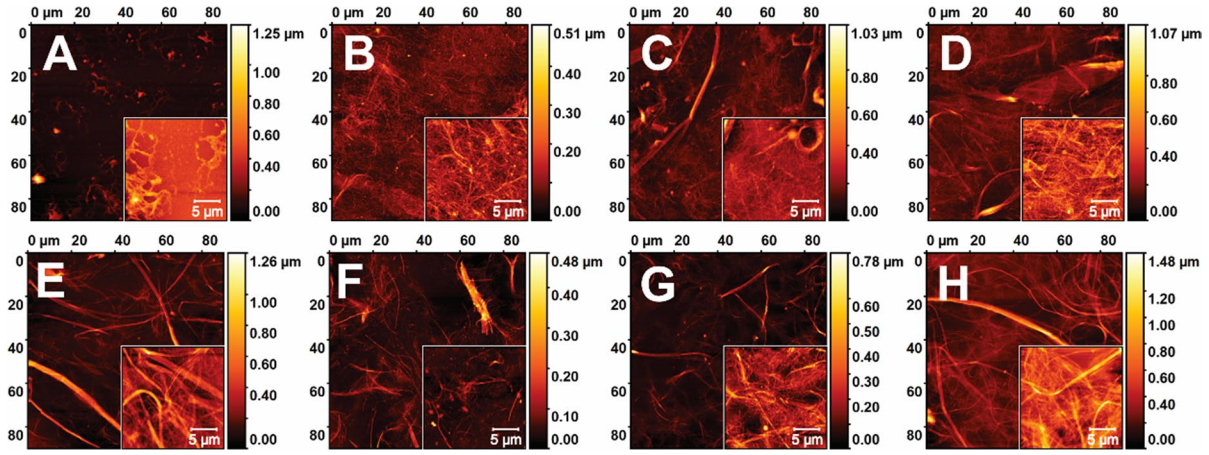

Fig. 1 AFM topographic images (90 µm × 90 µm) of **A** Control, **B** 1 cycle, **C** 3 cycles, **D** 6 cycles, **E** 12 cycles, **F** 15 cycles, **G** 18 cycles, and **H** 21 cycles. The insets in the lower right side of the images correspond to 20 µm × 20 µm AFM micrographs

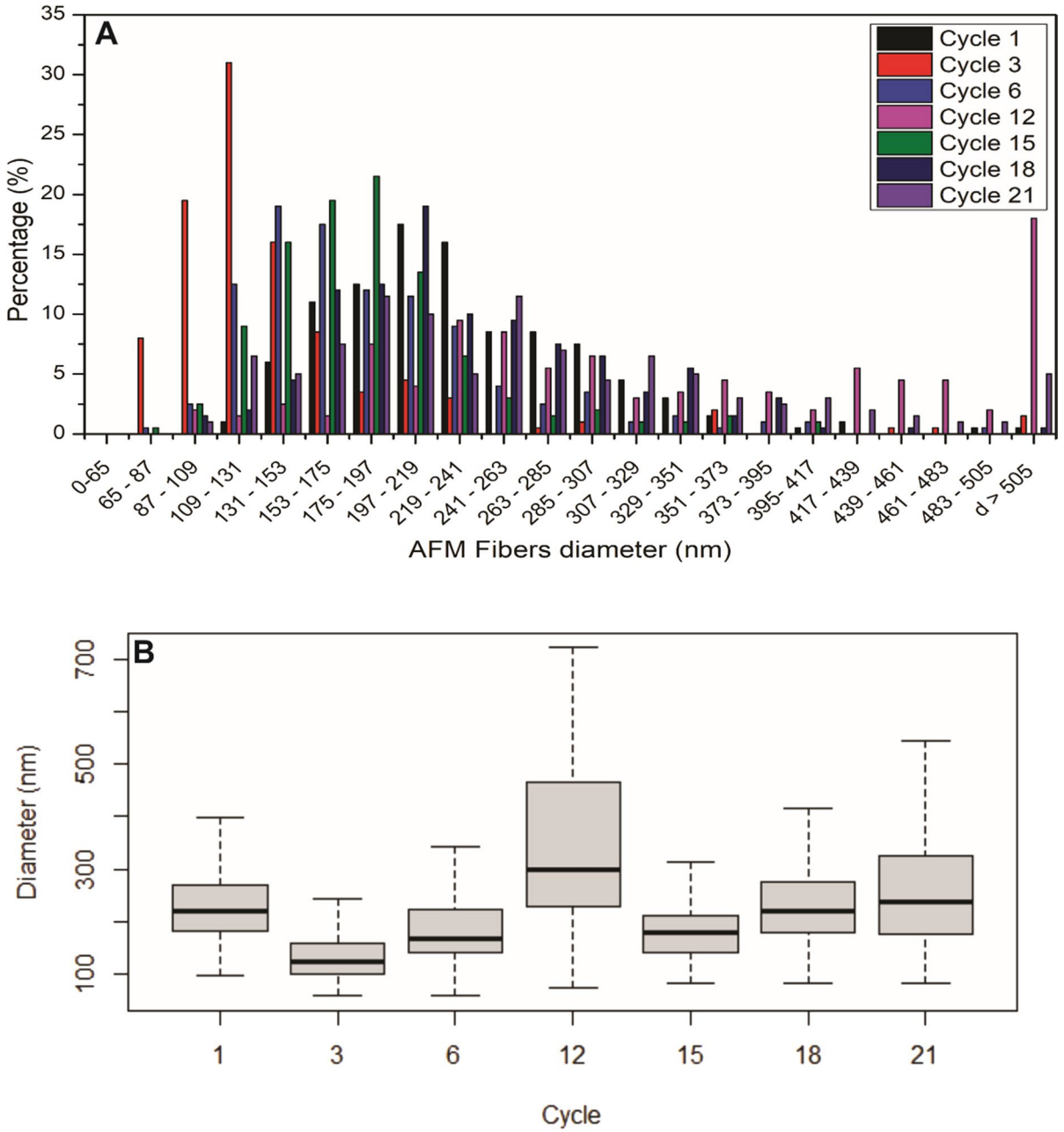

Fig. 2 Size distribution of CMFs in AFM **A** Histogram for fibers size diameter distribution and **B** Boxplot for mean diameter and standard deviation visualization (atypical points in the boxplot were excluded)

No size changes were observed for CMFs (see Fig. 2B). However, the studies of Larsson et al. (2019) have reported that the cellulose thicker fibers are composed of thinner fibers (Larsson et al. 2019). Further, the authors also confirmed the presence of a highly heterogeneous particle size distribution. Accordingly, vegetal cellulose can be described as a complex multiscale-constitute material where smaller fractions of fibers shape the thicker ones, which are observed in AFM micrographs (Chinga-Carrasco 2011). Hence, the generation of heterogeneous micro-/nanofibrils suspensions, from micrometer

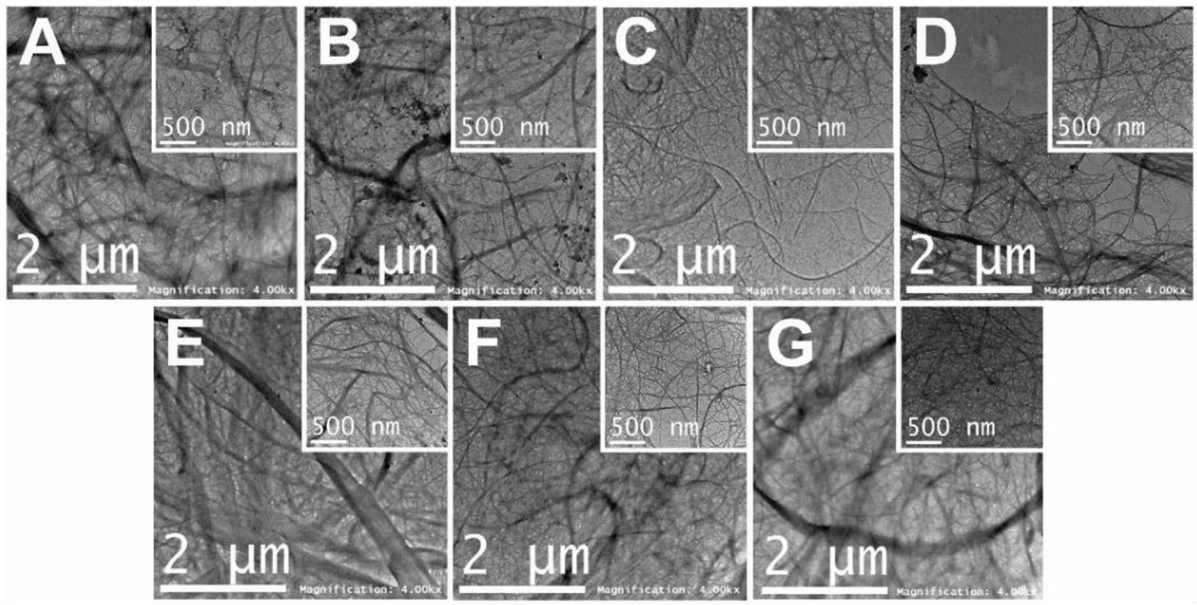

Fig. 3 TEM images of CMF and CNF morphology and size of **A** 1 cycle, **B** 3 cycles, **C** 6 cycles, **D** 12 cycles, **E** 15 cycles, **F** 18 cycles, and **G** 21 cycles at 4000X; the scale bar represents 2 µm. The insets in the upper right side of the images correspond to 9.900X; the scale bar represents 500 µm

to nanometer fiber diameters with some residual of non-delaminated fiber fragments (millimetric fibers), are generally present in physical treatments involving cellulose (Lehmonen et al. 2017; Berto and Arantes 2019).

Hence, the size variability in AFM analysis is related to the effect of mechanical fibrillation on the progressive breaking down of the hydrogen bonds and the cell wall structure, resulting in a mixture of fibrillated cellulose but also aggregates and entangled networks (Yuan et al. 2021). Herein, it is essential to consider that during the obtention of CNFs, a complex mix containing fibers, poorly fibrillated, and nanofibers in the millimeter, micrometer, and nanometer scale, respectively, or even oligomers in suspension, is produced. Thus, defining a "degree of fibrillation" is challenging, and multi-criteria methods with different resolutions are needed to analyze more than only a small fraction of a sample (Chinga-Carrasco 2013).

Therefore, a deeper analysis of CNFs was accomplished using TEM. The control sample was not characterized by TEM due to the large fiber size. The TEM images (see Fig. 3) confirmed the presence of CNFs during the homogenization process. The micrographs in Fig. 3 were representative images of the morphology and distribution of the defibrillated cellulose.

As the cycles increased, it was possible to visualize a decrease in the size diameter of the fibers from Fig. 3B (3 cycles) to Fig. 3G (21 cycles). These TEM micrographs allowed better visualization of CNFs compared to AFM micrographs and their dispersion in the dried state. Besides, thinner fibers and a high density of bent structures were also evidenced.

Moreover, once the diameters were plotted in Fig. 4A, the distribution also showed positively skewed data with the majority of the fiber population below 100 nm. In Fig. 4B, the boxplot evidenced a decrease in the mean diameter as the cycles increased. From a high number of cycles, the diameter of the corresponding fiber size was 17.18, 12.60, and 18.00 nm for 15, 18, and 21 cycles, respectively. Moreover, the non-parametric Kruskal–Wallis test showed a P-value $< 2.2e{-}16$, leading to the conclusion that not all group medians are equal (Ang et al. 2020).

It is important to highlight the novelty of the present approach, as the homogenizing and dispersant media is PG, contrary to other studies where

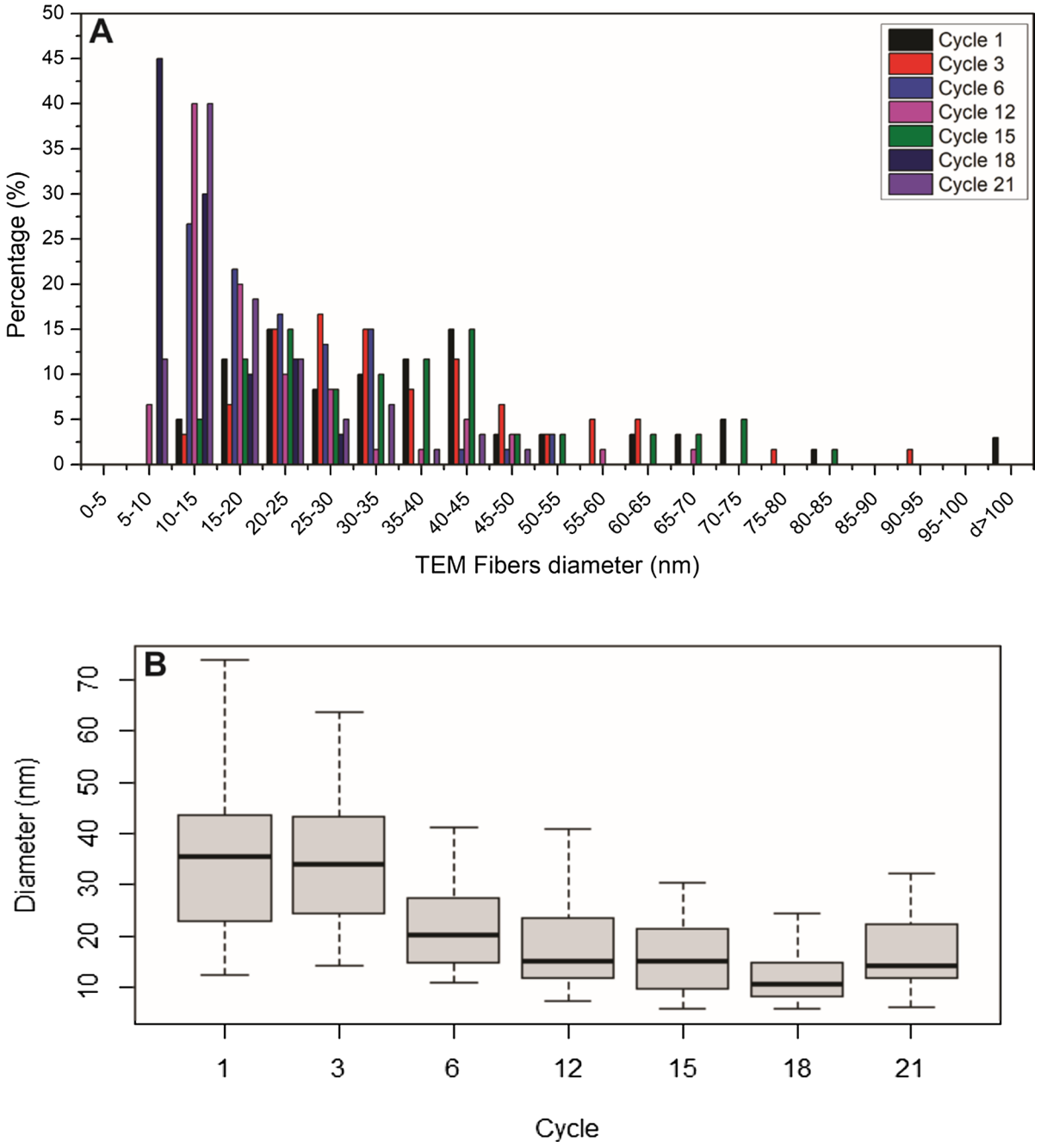

Fig. 4 Size distribution of CMFs and CNFs in TEM. **A** Histogram for fibers size diameter distribution and **B** Boxplot for mean diameter and standard deviation (typical points in the boxplot were excluded)

the slurry in the process is generally a diluted aqueous cellulose fiber suspension (0.5–1% p/p) (Djafari Petroudy et al. 2021). Accordingly, PG is an appropriate solvent for mechanical homogenization of vegetable cellulose.

Hence, the progressive presence of fibers in the nanoscale confirms that the CMFs were composed of smaller CNFs in a hierarchical and multiscale system, as has been widely reported in the literature (Chinga-Carrasco 2011).

Table 1 Behavior of CNF diameter evaluated with TEM. Control fibers were not included in the TEM analysis due to the large size of the fibers

Cycle	CNF mean diameter (nm)	Standard deviation (nm)	d < 15 nm (%)	d < 30 nm (%)	d < 60 nm (%)
1	38.57	21.17	5.00	40.00	83.33
3	36.36	15.74	3.33	41.67	91.67
6	22.55	9.68	26.67	78.33	100.00
12	20.06	12.53	46.67	85.00	98.33
15	17.18	9.44	50.00	93.33	100.00
18	12.60	5.70	75.00	100.00	100.00
21	18.00	9.28	51.67	86.67	100.00

Moreover, in the present study, the size diameter and standard deviation decrease with the number of cycles (see Table 1). And the percentage of fibers under 15 nm, 30 nm, and 60 nm rose as the number of cycles increased, leading to a smaller fiber population, as shown in Table 1. This indicates a trend for CNF homogenization with increasing cycles of mechanical treatment (Andrade et al. 2021).

Similarly, Table 1 also showed that the percentages of fiber < 60 nm result from more severe treatments. This cycle number-dependent behavior was explicit from 3 to 15 cycles, where most of the fibers reached nanometer dimensions. Contrary to subsequent cycles, which seemed not to affect the size of the homogenized vegetal cellulose.

This aligns with the studies of Andrade et al. (2021), who in a study employing high-pressure homogenization in *Eucalyptus* and *Pinus* to deconstruct cellulose nanofibers, reported a decrease in fiber diameter as the mechanical cycles increased. In that study, after 15 passes or cycles, the width of *Eucalyptus* fibers reached 16 nm on the nanometer scale, whereas *Pinus radiata* showed larger diameters (approximately 30 nm).

Likewise, one of the first works on the production of CNFs under 100 nm was carried out using high-pressure homogenization in a Manton–Gaulin Homogenizer with a wood pulp suspension (2 wt%) (Turbak et al. 1983). Thus, through the same mechanical process but using PG as defibrillation media instead of water, the presence of fibers below 100 nm was confirmed in this study. Other studies for homogenizing *Pinus Radiata* through aqueous media reported nanofibers diameters of around 3–50 nm (Iwamoto et al. 2007; Zimmermann et al. 2010; Tarrés et al. 2020; Andrade et al. 2021; Djafari Petroudy et al. 2021).

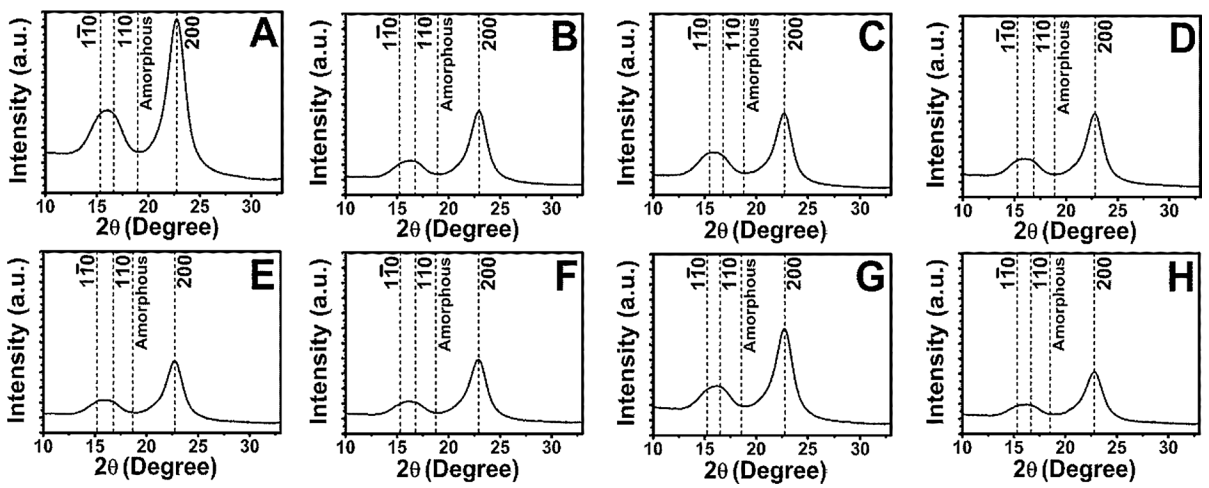

Fig. 5 XRD spectra of **A** control sample, **B** 1 cycle, **C** 3 cycles, **D** 6 cycles, **E** 12 cycles, **F** 15 cycles, **G** 18 cycles, and (H) 21 cycles

Hence, the presence of PG in the process enabled defibrillation, which behaves similarly to aqueous systems while contributing as a glycol-based-dispersant agent (Liang et al. 2008). Likewise, PG could act as a stabilizing agent avoiding the hornification process of CMFs and CNFs into bigger bundles, which is the irreversible collapse of cellulose fibers from the swollen to the dehydrated state (Ding et al. 2019). Therefore, stabilization can be related to the hydrophilic nature of PG acting as a media and participating in the defibrillation, considering that the agglomeration of chains would be difficult to destroy during the mix with a highly hydrophobic matrix (Canché-Escamilla et al. 2002; Pandey et al. 2015).

Complementary morphological analysis was performed using X-ray crystallography. Thus, Fig. 5 shows the diffractograms of fibrillation samples during the different cycles. All samples exhibit specific peaks and intensities related to cellulose type I from 10° to 35° using X-ray diffraction. It also shows three common peaks of crystallographic planes defined at ($1\underline{1}0$), (110), and (200) (Poletto et al. 2014; French 2014). And the amorphous region was defined at 2θ between 18 and 22° (Zuluaga et al. 2009; Poletto et al. 2014; Ahvenainen et al. 2016). Furthermore, the overlapping between $1\underline{1}0$ and 110 indicates that the structure corresponds to cellulose I, which is a mixture of celluloses Iα (triclinic) and Iβ (monoclinic) (Shankaran 2018). The crystallinity degree ranged from 68 to 75%. These results are consistent with reported values.

On the other hand, Sanchez-Salvador et al. (2021) evaluated different nanofibrillation yields with five pressure sequences (PS). After two wood-based pulps (Eucalyptus and Pine) were pretreated, this mechanical treatment was achieved using five PS in an aqueous solution. It started from less intensive to more intensive high-pressure homogenization, with different quantities of passes or cycles. As a result, the Eucalyptus and Pine fibers presented crystallinity indexes of 72.7% and 78.3%, respectively (Sanchez-Salvador et al. 2021), as obtained herein.

Nevertheless, some reports state that the number of cycles causes decreases in the crystallinity index due to the constant shear rate during the fibrillation process in water media (Sharma et al. 2015; He et al. 2018). Hence, a slight depletion of the crystallinity index was observed as homogenization cycles increased up to 21, in which crystallinity was 68%. Still, according to Table 2, when vegetable cellulose is homogenized in PG, no remarkable reduction of crystallinity with the number of cycles takes place; this is an advantage for further applications of nanocellulose.

Mechanical treatment, compared to water, did not alter the crystal organizations notably due to the lower polarity of PG (Wang et al. 2019), which could prevent the hydrogen bonding from breaking and which is linked to the amorphization of cellulose fibers during homogenization processes. Furthermore, the control sample presented an initial crystallinity of 76.46%. Thus, PG provides OH groups that could participate in hydrogen bonding interactions with reactive OH groups, abundant on the CNF surfaces.

Moreover, PG is a bigger molecule compared to water, with higher viscosity and lower dielectric constant (Wang et al. 2019). These last characteristics may influence the dispersion quality, which could lead to preserving crystalline regions that act as lubricants through OH interactions during the mechanical process (Özdemir and Nofar 2021).

Consequently, hydrogen bonds might be responsible for keeping the linear cellulose chains arranged in sheets. At the same time, stacking the sheets into the

Table 2 Average crystallinity percentages (% C), interplanar distances (d), and apparent crystal size (ACS) were identified for morphological analysis according to the homogenization cycle

Cycle Number	% C	$1\bar{1}0$		110		200	
		d (nm)	ACS (nm)	d (nm)	ACS (nm)	d (nm)	ACS (nm)
1	74.77	0.58	4.64	0.53	4.97	0.39	4.51
3	73.22	0.58	3.83	0.53	5.10	0.39	4.75
6	72.72	0.58	4.79	0.53	4.88	0.39	4.50
12	71.81	0.58	4.96	0.53	5.27	0.39	4.36
15	71.67	0.58	5.55	0.53	4.27	0.39	4.26
18	72.65	0.58	4.45	0.53	4.79	0.39	4.41
21	68.45	0.58	5.04	0.53	4.44	0.39	4.29

three-dimensional crystal structures of the cellulose material involves hydrophobic interactions. Therefore, it has been suggested that hydrophobic interactions contribute favorably to stabilizing a crystal-like stacked structure (Bergenstråhle et al. 2010; Olsson and Westman 2013).

It is evidenced in Table 2 that the interplanar distances and apparent crystal size belonging to the three reflections do not present significant changes. These results also support the idea related to no substantial changes in crystallite size occurring during the cycles of mechanical treatment. Also, it has been previously reported that the size of cellulose crystal is approximately 5 nm in width (Park et al. 2010), coherent with the findings of Table 2 about the results of such value.

Further, the interplanar spacing (d-spacing) has been attributed to crystallite size variations of CNFs. Therefore, the d-spacing values found in this study for the three crystallographic planes ($1\bar{1}0$, 110, and 200) are 0.58, 0.53, and 0.39 nm, which are close to the reported values (Wada et al. 2001; Ioelovich 2017).

Reported studies (Rambabu et al. 2016) that applied a mechanical process indicate no significant reduction in crystal size (around 4 nm), even after increasing grinding passes from 0 to 12, as was also evidenced in this study. Based on this, PG is a suitable, practical, and non-destructive route when the original characteristics of the cellulose crystallinity are required. It preserves the crystal size, interplanar distances, and the mechanical cycles with an in situ organic media fibrillation and dispersion process.

Moreover, the results of Table 2 show no impact of the mechanical cycles in CMF and CNF ACS in the presence of PG, likewise crystallinity and interplanar distances did not evidence changes between cycles. This performance is relevant given that the fibers' intrinsic properties were not lost while the morphological dimensions decreased, thus contributing to potentially better properties related to the nanoscale. Hence, adding PG to the defibrillation process is a suitable pathway for the non-water homogenization process.

Chemical analysis

FTIR spectroscopy was also used to establish variations in the chemical structure of the cellulose fibers resulting from the number of cycles. Results are shown in Fig. 6.

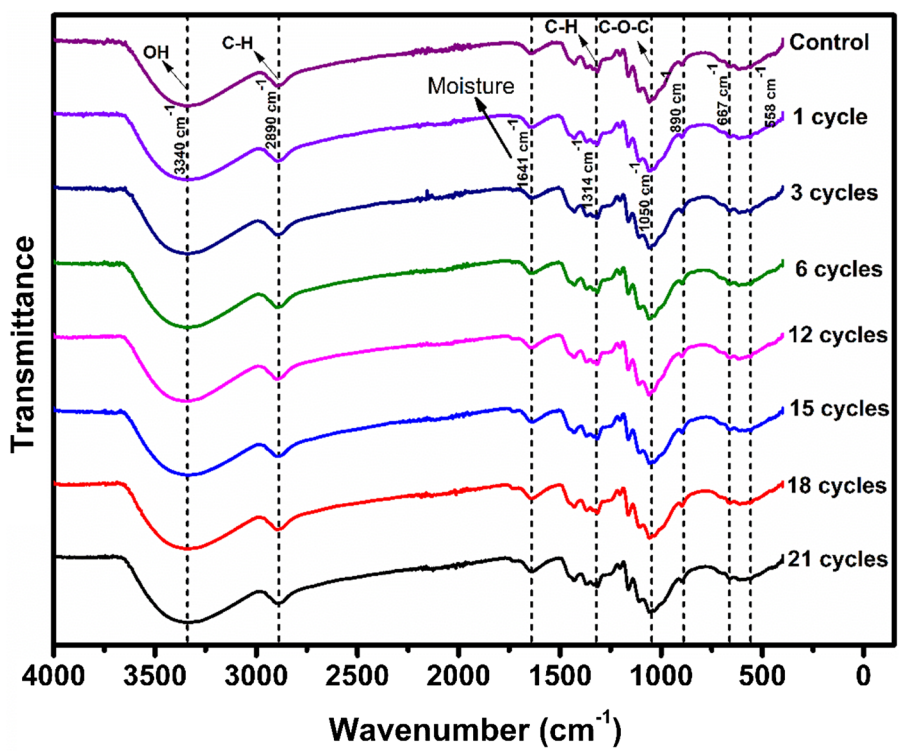

Fig. 6 FTIR spectra for different cellulose cycles in PG of the control sample. 1, 3, 6, 12, 15, 18, and 21 cycles with their characteristic vibrations

Native cellulose (control) had a broadened band of the OH-stretching around 3650–3000 cm^{-1} (centered in 3340 cm^{-1}). This is evidenced in all spectra of Fig. 6, given the OH group contribution in the cellulose and the PG. The OH groups in both molecules enabled the inter- and intramolecular hydrogen bond formation. The vibration at 2890 cm^{-1}, resulting from the C–H stretching vibration, corresponds to the hybridization of C_{sp3} in the methyl group of PG. And the band with weak intensity centered at 1641 cm^{-1} is potentially related to the OH vibration of the absorbed water.

Further, in all seven treatments, the band near 1050 cm^{-1} corresponds to C–O–C at the pyranose ring of cellulose (Cichosz and Masek 2020). The bands at 1429, 1314, 1203, and 1162 cm^{-1}, as reported by similar values, are characteristic of C–H, C–O deformation, bending, or stretching vibrations of many groups in carbohydrates (Poletto et al. 2014).

The 896 cm^{-1} band in the spectra corresponds to β-glycosidic links between the glucose units of cellulose, as has been reported (Benini et al. 2018). Whereas the band centered between 667 and 558 cm^{-1} corresponds to CH deformation and OH out-of-plane bending (Li and Renneckar 2011).

The seven spectra did not show appreciable changes in FTIR spectra throughout the progressive cycles (Velásquez-Cock et al. 2016). Accordingly, the mechanical stress does not affect the cellulose's chemical conformation, which is probably only disaggregated through intermolecular bonding ruptures.

Moreover, the intensity of the OH characteristic band located at 3340 cm^{-1}, useful for identifying changes in the intermolecular interactions, did not show substantial changes (Persson et al. 1991). This behavior could also be due to the presence of native OH groups of the cellulose.

The band located at 1030 cm^{-1} has been related to hemicellulose, ligneous structures, and cellulose I (Zuluaga et al. 2009; Velásquez-Cock et al. 2016). Hence, the presence of this band (centered at 1050 cm^{1}) confirms the presence of cellulose type I.

Furthermore, in the fingerprint region, the bands between 900 and 800 cm^{-1} help to identify the α and β configuration of anomeric carbon. Hence, it has been reported that cellulose with 1,4-β-D-glucopyranose, as a building block with a β anomeric carbon configuration, shows a band of around 890 cm^{-1} confirming the existence of β configuration (Hong et al. 2021).

It has also been reported that the ratio between the 710/3240 and 750/3270 cm^{-1} bands are typical of cellulose crystalline allomorphs: I_α and I_β (Šturcova et al. 2004; Horikawa and Sugiyama 2009; Osorio et al. 2019). The ratio of the two phases critically depends on the cellulose origin (Heiner et al. 1995). Hence, the absorbance's integral area related to the bands at 710 and 750 cm^{-1} was calculated. The mean area of 710 cm^{-1} bands for 1 to 21 cycles concerning the predominant I_β allomorph was 0.9718 with a standard deviation of 0.0721. This result supports the XRD findings, where no changes in the nanocellulose's crystallinity or its crystal type were evidenced along with the fibrillation cycles.

To summarize, the fibrillation in the presence of PG and its effect, once it has been evaporated, does not impact the β anomeric carbon configuration of cellulose, even if the number of cycles increases. Further, it can be stated that, in a fresh sample, the abundant OH groups in the hydrophilic PG will form hydrogen bonds through inter- and intra-molecular interactions across the fibers interface, as proposed in Fig. 7. However, once removed, the chemical conformation of cellulose is kept.

Thermal analysis

The thermal degradation of the control sample and the homogenized nanocellulose in PG as solid films is illustrated in Fig. 8.

Figure 8A shows that all samples had a similar behavior characterized by two thermal events based on the non-processed sample (control). The PG thermogram is shown in Figure S2. The first weight-loss event is below 100 °C and relates to moisture release. And the main thermal event presented at 225 °C relates to hemicelluloses depolymerization overlapped with cellulose decomposition at 350 °C in the maximum rate of decomposition (Poletto et al. 2012; Velásquez-Cock et al. 2016; Nurazzi et al. 2021). Therefore, the results suggest that the number of mechanical cycles does not affect the thermal properties of materials in the dried state, confirming the stabilizing effect of PG.

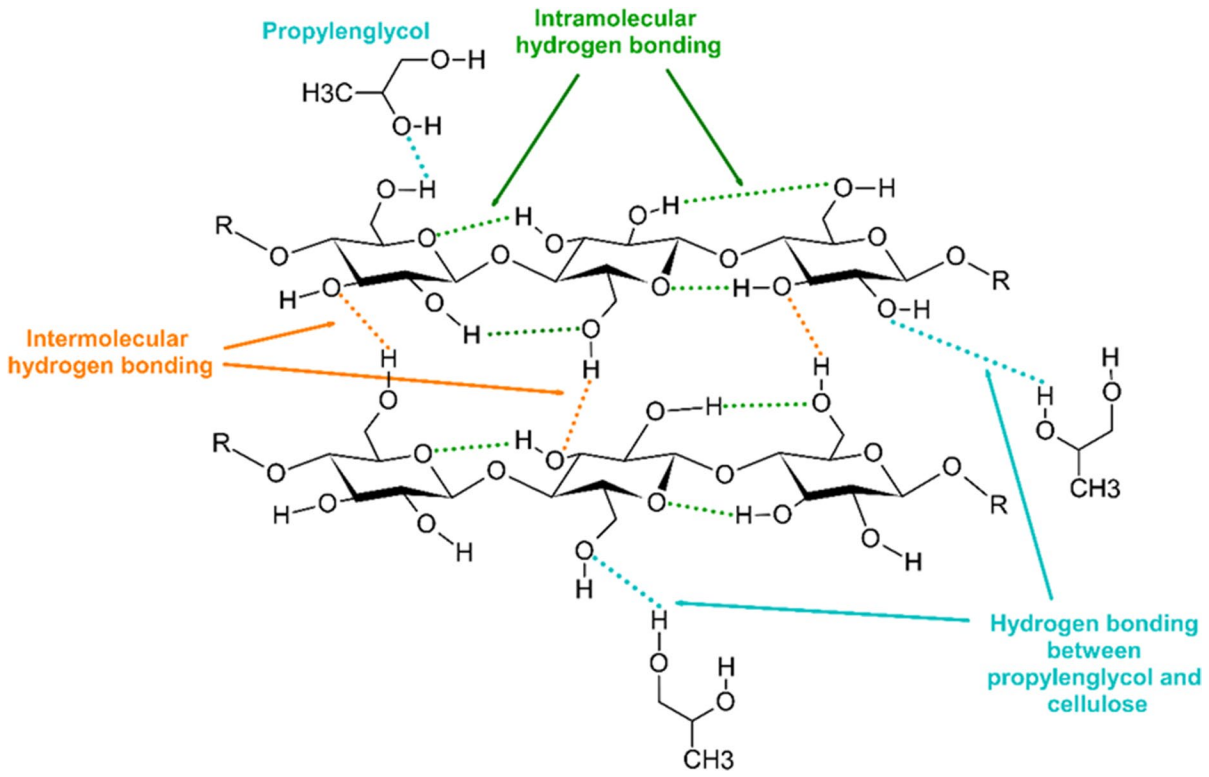

Fig. 7 Schematic representation of a cellulose section and PG interactions through OH groups

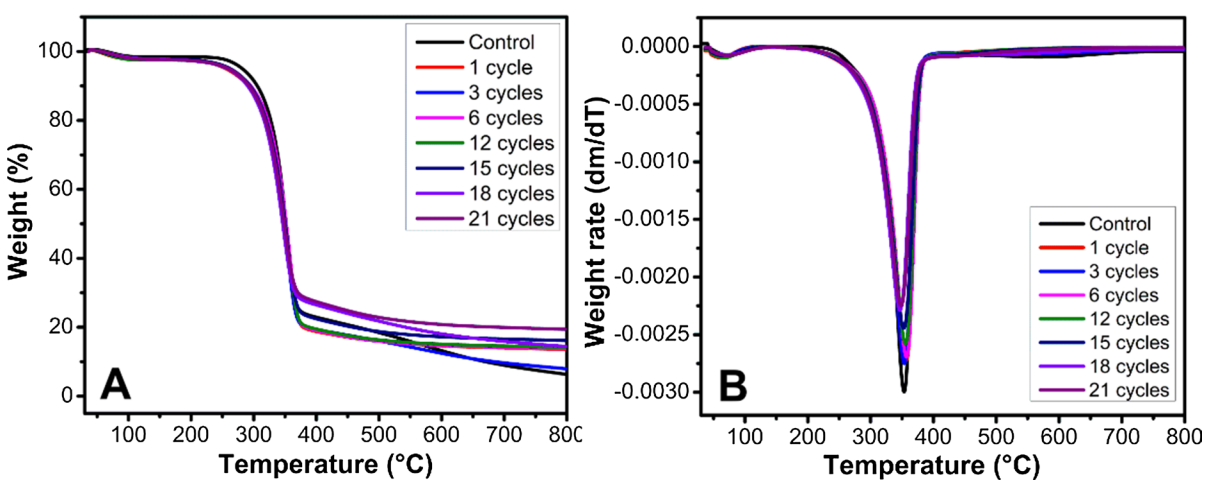

Fig. 8 Thermal behavior of homogenized vegetable nanocellulose in PG. **A** Thermal degradation plots and **B** Derivative thermograms of the control and 1, 3, 6, 9, 12, 15, 18, and 21 cycles

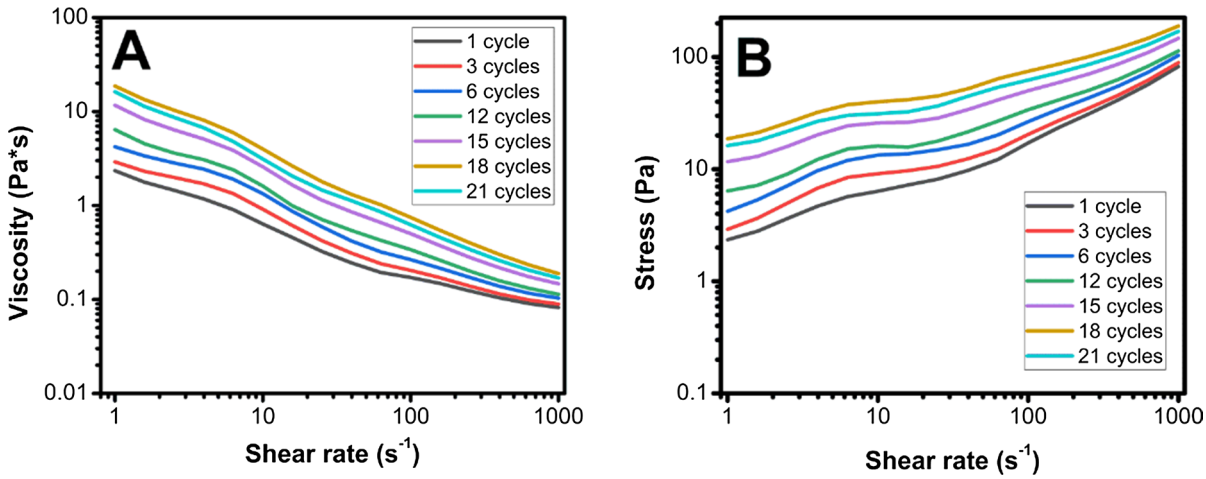

Fig. 9 Rheological behavior of homogenized vegetable nanocellulose in PG **A** Shear-thinning behavior and **B** flow curve of CNFs suspensions in PG

Shear flow properties

Figure 9A shows a shear-thinning behavior of CNF suspensions. Interestingly, as the homogenization cycles increased, the initial viscosity was higher, followed by a decreasing behavior in all cycles, which has a similar viscosity profile as reported in the literature (Nechyporchuk et al. 2016). The shear-thinning behavior was also verified through the Power Law Equation, confirming an $n < 1$ (pseudoplastic) (Sheng 2011) for all the cycles (See supplementary information, Table S1). This is related to the surface area growth followed by increased interactions among hydrogen bonds. Subsequently, the viscosity in every cycle decreased as the shear rate increased due to the microscale structural rearrangements within the suspension with glycol (Wang et al. 2019).

Furthermore, the shear flow performance can be useful for studying the degree of fibrillation. For example, Herrick et al. (1983) and Grüneberger et al. (2014) analyzed the viscosity of CNFs obtained through mechanical fibrillation, finding an increase in viscosity as the number of passes or cycles in the homogenizer and grinder rose, respectively.

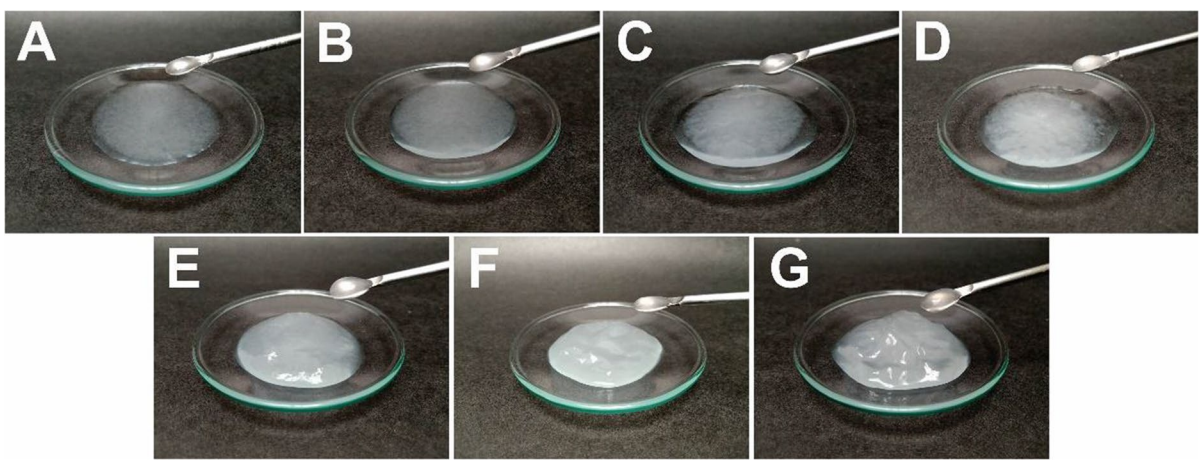

Fig. 10 The visual appearance of fibrillated cellulose in PG. **A** 1 cycle, **B** 3 cycles, **C** 6 cycles, **D** 12 cycles, **E** 15 cycles, **F** 18 cycles, and **G** 21 cycles

As detected in the morphology characterization, there was a decrease in the fiber's diameter, especially from 3 to 12 cycles (from 15 to 21 cycles, the diameter was not significantly reduced), which may affect the viscosity. For all the cycle samples, the decreasing viscosity phenomenon with the shear rate relates to the growing disentanglement of fibers in the suspension during the mechanical process and the humectation with PG, causing a shear-induced structure (Wang et al. 2019). Herein, in Fig. 7A the flow behavior in the lower shear region (below 10 s^{-1}) is remarkably different. In contrast, in the shear region upper 100 s^{-1}, the viscosity's trend for the seven treatments (cycles) starts to come close to each other.

As indicated by TEM and AFM measurements, the CMF and CNF diameter were significantly reduced as the number of mechanical cycles increased. This behavior also affected the rheological performance. Thus, with the progressive homogenization of vegetable cellulose, the surface charge of the fibrils was improved. This increased fiber area, and contact points were available to entrap the PG surrounding media. The combination of immobilized PG on the cellulose surface and PG in the interfibrillar spacing produces fibrillar matrices with a gel-like behavior (Ang et al. 2019), whose apparent thickening increases as the number of cycles rises. Hence, the information found through the rheological analysis was visually confirmed (Fig. 10), where phase separation is evidenced in the first cycles due to the major presence of CMFs and the lack of homogenized fibers (Nechyporchuk et al. 2016). At upper cycles, there is an apparent increase in the initial viscosity and no evidence of phase separation. The above is congruent with what was found in the viscosity performance.

Conclusions

In this study, the high-pressure homogenization with PG treatment influenced the diameter of vegetal cellulose fibers. However, it has been widely reported that mechanically derived nanocellulose is still challenging to process and characterize. The mechanical processes did not significantly change the crystallinity of the samples, and it preserved features such as the apparent crystal size and the interplanar spacing due to the PG-cellulose hydrogen bonding interactions.

Furthermore, the chemical composition of the CMFs and CNFs, according to the spectroscopy analysis, exposed to different grinding cycles, did not present changes. Moreover, the effect of the mechanical homogenization in the fibers' diameters was evidenced by the subsequent study of rheological behavior, showing a shear-thinning behavior with PG as a non-toxic water-free media, as previously reported in aqueous media. Therefore, mechanical methods for cellulose fibrillation, compared to functionalization or solvent exchange, present interesting advantages as they do not require complex conditions and do not cause pollution problems, making them easier to industrialize. Further, high-pressure homogenization is also environmentally friendly, compared to chemical treatment techniques, while preserving the most important properties of cellulose micro-/nanofibers and avoiding implementing toxic solvents. Then, this study proposes a route for the processing and sustainable obtention of CMFs and CNFs simultaneously dispersed in a water-free media as potential reinforcing materials, which may even be compatible with the widely employed less-hydrophilic matrices.

Author contributions EHB wrote the paper; MO oriented and supervised the work; and CC got the funding and supervised the writing and analysis. In addition, EHB, MO, DM, PG, MP, DB, and CC participated in the characterization and discussion. Finally, DM, PG, MP, DB, and CC reviewed and approved the manuscript.

Funding Open Access funding provided by Colombia Consortium. The authors want to thank MINCIENCIAS for funding the project *via* the followings grants. E. Hernández-Becerra thanks to The *Iniciativa Jóvenes Talento* (Young Talents Initiative) under the grant number APSC 854-2020 (MINCIENCIAS, Colombia), and D. Marín likes to thank to the grant numbrer 758-2016 (MINCIENCIAS, Colombia). Furthermore, the authors thank to Andercol-Akzonobel for the technical assistance in the project.

Declarations

Conflict of interest The authors have no relevant financial or non-financial interests to disclose.

References

Ahvenainen P, Kontro I, Svedström K (2016) Comparison of sample crystallinity determination methods by X-ray diffraction for challenging cellulose I materials. Cellulose 23:1073–1086. https://doi.org/10.1007/S10570-016-0881-6

Amara C, El Mahdi A, Medimagh R, Khwaldia K (2021) Nanocellulose-based composites for packaging applications. Curr Opin Green Sustain Chem 31:100512. https://doi.org/10.1016/J.COGSC.2021.100512

Andrade A, Henríquez-Gallegos S, Albornoz-Palma G, Pereira M (2021) Effect of the chemical and structural characteristics of pulps of Eucalyptus and Pinus on the deconstruction of the cell wall during the production of cellulose nanofibrils. Cellulose 28:5387–5399. https://doi.org/10.1007/s10570-021-03848-0

Andrade A (2022) Aplicación de enzimas y nanocelulosa en la industrial del papel reciclado: análisis de indicadores de proceso y de ecoeficiencia. Universidad de Concepción

Ang S, Haritos V, Batchelor W (2019) Effect of refining and homogenization on nanocellulose fiber development, sheet strength and energy consumption. Cellulose 26:4767–4786. https://doi.org/10.1007/s10570-019-02400-5

Ang S, Narayanan JR, Kargupta W et al (2020) Cellulose nanofiber diameter distributions from microscopy image analysis: effect of measurement statistics and operator. Cellulose 27:4189–4208. https://doi.org/10.1007/S10570-020-03058-0/TABLES/7

Ansell MP (2015) Wood microstructure—a cellular composite. In: Wood composites. Elsevier, pp 3–26

Bangar SP, Whiteside WS (2021) Nano-cellulose reinforced starch bio composite films—a review on green composites. Int J Biol Macromol 185:849–860. https://doi.org/10.1016/j.ijbiomac.2021.07.017

Barhoum A, Li H, Chen M, et al (2019) Emerging applications of cellulose nanofibers. In: Handbook of nanofibers. Springer, pp 1131–1156

Benini KCC, Voorwald HJC, Cioffi MOH et al (2018) Preparation of nanocellulose from Imperata brasiliensis grass using Taguchi method. Carbohydr Polym 192:337–346. https://doi.org/10.1016/j.carbpol.2018.03.055

Bergenstråhle M, Wohlert J, Himmel M, Brady J (2010) Simulation studies of the insolubility of cellulose. Carbohydr Res 345:2060–2066. https://doi.org/10.1016/J.CARRES.2010.06.017

Berto GL, Arantes V (2019) Kinetic changes in cellulose properties during defibrillation into microfibrillated cellulose and cellulose nanofibrils by ultra-refining. Int J Biol Macromol 127:637–648. https://doi.org/10.1016/j.ijbiomac.2019.01.169

Builes DH, Labidi J, Eceiza A et al (2013) Unsaturated polyester nanocomposites modified with fibrillated cellulose and PEO-b-PPO-b-PEO block copolymer. Compos Sci Technol 89:120–126. https://doi.org/10.1016/j.compscitech.2013.09.015

Canché-Escamilla G, Rodriguez-Laviada J, Cauich-Cupul JI et al (2002) Flexural, impact and compressive properties of a rigid-thermoplastic matrix/cellulose fiber reinforced composites. Compos Part A Appl Sci Manuf 33:539–549. https://doi.org/10.1016/S1359-835X(01)00136-1

Carpita NC, Gibeaut DM (1993) Structural models of primary cell walls in flowering plants: consistency of molecular structure with the physical properties of the walls during growth. Plant J 3:1–30. https://doi.org/10.1111/j.1365-313X.1993.tb00007.x

Chanda S, Bajwa DS (2021) A review of current physical techniques for dispersion of cellulose nanomaterials in polymer matrices. Rev Adv Mater Sci 60:325–341. https://doi.org/10.1515/rams-2021-0023

Chinga-Carrasco G (2011) Cellulose fibres, nanofibrils and microfibrils: the morphological sequence of MFC components from a plant physiology and fibre technology point of view. Nanoscale Res Lett 6:1–7. https://doi.org/10.1186/1556-276X-6-417

Chinga-Carrasco G (2013) Optical methods for the quantification of the fibrillation degree of bleached MFC materials. Micron 48:42–48. https://doi.org/10.1016/j.micron.2013.02.005

Cichosz S, Masek A (2020) IR study on cellulose with the varied moisture contents: Insight into the supramolecular structure. Materials (basel) 13:1–22. https://doi.org/10.3390/ma13204573

de Souza AG, Rocha DB, Kano FS, dos Rosa D (2019) Valorization of industrial paper waste by isolating cellulose nanostructures with different pretreatment methods. Resour Conserv Recycl 143:133–142. https://doi.org/10.1016/j.resconrec.2018.12.031

Desmaisons J, Boutonnet E, Rueff M et al (2017) A new quality index for benchmarking of different cellulose nanofibrils. Carbohydr Polym 174:318–329. https://doi.org/10.1016/J.CARBPOL.2017.06.032

Ding Q, Zeng J, Wang B et al (2019) Effect of nanocellulose fiber hornification on water fraction characteristics and hydroxyl accessibility during dehydration. Carbohydr Polym 207:44–51. https://doi.org/10.1016/J.CARBPOL.2018.11.075

Djafari Petroudy SR, Chabot B, Loranger E et al (2021) Recent advances in cellulose nanofibers preparation through energy-efficient approaches: a review. Energies 14:6792

Dufresne A (2019) Nanocellulose processing properties and potential applications. Curr Rep 5:76–89. https://doi.org/10.1007/s40725-019-00088-1

Dufresne A (2008) Cellulose-based composites and nanocomposites. In: Monomers, polymers and composites from renewable resources. Elsevier, pp 401–418

Ferreira DP, Cruz J, Fangueiro R (2018) Surface modification of natural fibers in polymer composites. In: Green composites for automotive applications. Elsevier, pp 3–41

French AD (2014) Idealized powder diffraction patterns for cellulose polymorphs. Cellulose 21:885–896. https://doi.org/10.1007/S10570-013-0030-4/FIGURES/5

French AD (2017) Glucose, not cellobiose, is the repeating unit of cellulose and why that is important. Cellulose 24:4605–4609. https://doi.org/10.1007/s10570-017-1450-3

French AD (2020) Increment in evolution of cellulose crystallinity analysis. Cellulose 27:5445–5448. https://doi.org/10.1007/s10570-020-03172-z

French AD, Santiago Cintrón M (2013) Cellulose polymorphy, crystallite size, and the Segal Crystallinity Index. Cellulose 20:583–588. https://doi.org/10.1007/s10570-012-9833-y

Grüneberger F, Künniger T, Zimmermann T, Arnold M (2014) Rheology of nanofibrillated cellulose/acrylate systems for coating applications. Cellulose 21:1313–1326. https://doi.org/10.1007/s10570-014-0248-9

Guan QF, Bin YH, Han ZM et al (2021) Plant cellulose nanofiber-derived structural material with high-density reversible interaction networks for plastic substitute. Nano Lett 21:8999–9004. https://doi.org/10.1021/ACS.NANOLETT.1C02315/SUPPL_FILE/NL1C02315_SI_001.PDF

He M, Yang G, Chen J et al (2018) Production and characterization of cellulose nanofibrils from different chemical and mechanical pulps. J Wood Chem Technol 38:149–158. https://doi.org/10.1080/02773813.2017.1411368

Heiner AP, Sugiyama J, Teleman O (1995) Crystalline cellulose Iα and Iβ studied by molecular dynamics simulation. Carbohydr Res 273:207–223. https://doi.org/10.1016/0008-6215(95)00103-Z

Herrick FW, Casebier RL, Hamilton JK, Sandberg KR (1983) Microfibrillated cellulose: morphology and accessibility. J Appl Polym Sci Appl Polym Symp 37:797–813

Hong T, Yin J-Y, Nie S-P, Xie M-Y (2021) Applications of infrared spectroscopy in polysaccharide structural analysis: progress, challenge and perspective. Food Chem X 12:100168. https://doi.org/10.1016/j.fochx.2021.100168

Horikawa Y, Sugiyama J (2009) Localization of crystalline allomorphs in cellulose microfibril. Biomacromol 10:2235–2239. https://doi.org/10.1021/bm900413k

Ioelovich M (2017) Characterization of various kinds of nanocellulose. In: Handbook of nanocellulose and cellulose nanocomposites. Wiley, pp 51–100

Iwamoto S, Nakagaito AN, Yano H (2007) Nano-fibrillation of pulp fibers for the processing of transparent nanocomposites. Appl Phys A Mater Sci Process 89:461–466. https://doi.org/10.1007/s00339-007-4175-6

Jiang Z, Tang L, Gao X et al (2019) Solvent regulation approach for preparing cellulose-nanocrystal-reinforced regenerated cellulose fibers and their properties. ACS Omega 4:2001–2008. https://doi.org/10.1021/acsomega.8b03601

Kaldéus T, Larsson PT, Boujemaoui A, Malmström E (2018) One-pot preparation of bi-functional cellulose nanofibrils. Cellulose 25:7031–7042. https://doi.org/10.1007/s10570-018-2066-y

Klemm D, Philipp B, Heinze T et al (1998) Comprehensive cellulose chemistry. Wiley

Larsson PA, Riazanova AV, Cinar Ciftci G et al (2019) Towards optimised size distribution in commercial microfibrillated cellulose: a fractionation approach. Cellulose 26:1565–1575. https://doi.org/10.1007/s10570-018-2214-4

Lee SY, Chun SJ, Kang IA, Park JY (2009) Preparation of cellulose nanofibrils by high-pressure homogenizer and cellulose-based composite films. J Ind Eng Chem 15:50–55. https://doi.org/10.1016/J.JIEC.2008.07.008

Lehmonen J, Pere J, Hytönen E, Kangas H (2017) Effect of cellulose microfibril (CMF) addition on strength properties of middle ply of board. Cellulose 24:1041–1055. https://doi.org/10.1007/s10570-016-1146-0

Li Q, Renneckar S (2011) Supramolecular structure characterization of molecularly thin cellulose i nanoparticles. Biomacromol 12:650–659. https://doi.org/10.1021/bm101315y

Li T, Chen C, Brozena AH et al (2021) Developing fibrillated cellulose as a sustainable technological material. Nature 590:47–56. https://doi.org/10.1038/s41586-020-03167-7

Liang S, Wu J, Tian H et al (2008) High-strength cellulose/poly(ethylene glycol) gels. Chemsuschem 1:558–563. https://doi.org/10.1002/cssc.200800003

Malachowska E, Dubowik M, Lipkiewicz A et al (2020) Analysis of cellulose pulp characteristics and processing parameters for efficient paper production. Sustain 12:7219. https://doi.org/10.3390/SU12177219

Mateo S, Peinado S, Morillas-Gutiérrez F et al (2021) Nanocellulose from agricultural wastes: products and applications—a review. Processes 9:1594. https://doi.org/10.3390/pr9091594

Medronho B, Romano A, Miguel MG et al (2012) Rationalizing cellulose (in)solubility: reviewing basic physicochemical aspects and role of hydrophobic interactions. Cellulose 19:581–587. https://doi.org/10.1007/s10570-011-9644-6

Mondal S (2018) Review on nanocellulose polymer nanocomposites. Polym Plast Technol Eng 57:1377–1391

Moon RJ, Martini A, Nairn J et al (2011) Cellulose nanomaterials review: structure, properties and nanocomposites. Chem Soc Rev 40:3941–3994. https://doi.org/10.1039/c0cs00108b

Nechyporchuk O, Belgacem MN, Pignon F (2016) Current progress in rheology of cellulose nanofibril suspensions. Biomacromol 17:2311–2320

Nurazzi NM, Asyraf MRM, Rayung M et al (2021) Thermogravimetric analysis properties of cellulosic natural fiber polymer composites: a review on influence of chemical treatments. Polymers (basel) 13:2710. https://doi.org/10.3390/POLYM13162710

Ogawa Y, Putaux JL (2019) Transmission electron microscopy of cellulose. Part 2: technical and practical aspects. Cellulose 26:17–34. https://doi.org/10.1007/s10570-018-2075-x

Oksman K, Aitomäki Y, Mathew AP et al (2016) Review of the recent developments in cellulose nanocomposite processing. Compos Part A Appl Sci Manuf 83:2–18. https://doi.org/10.1016/j.compositesa.2015.10.041

Olsson C, Westman G (2013) Direct dissolution of cellulose: background, means and applications. Cellul Fundam Asp. https://doi.org/10.5772/52144

Omran AAB, Mohammed AABA, Sapuan SM et al (2021) Micro-and nanocellulose in polymer composite materials: a review. Polymers (basel) 13:1–30

Osong SH, Norgren S, Engstrand P (2016) Processing of wood-based microfibrillated cellulose and nanofibrillated cellulose, and applications relating to papermaking: a review. Cellulose 23:93–123. https://doi.org/10.1007/s10570-015-0798-5

Osorio M, Fernández-Morales P, Gañán P et al (2019) Development of novel three-dimensional scaffolds based on bacterial nanocellulose for tissue engineering and regenerative medicine: effect of processing methods, pore size, and surface area. J Biomed Mater Res Part A. https://doi.org/10.1002/jbm.a.36532

Özdemir B, Nofar M (2021) Effect of solvent type on the dispersion quality of spray-and freeze-dried CNCs in PLA through rheological analysis. Carbohydr Polym 268:118243. https://doi.org/10.1016/j.carbpol.2021.118243

Pandey JK, Takagi H, Nakagaito AN, Kim HJ (2015) Handbook of polymer nanocomposites. Processing, performance and application: volume C: polymer nanocomposites of cellulose nanoparticles. Springer, Berlin

Park S, Baker JO, Himmel ME et al (2010) (2010) Cellulose crystallinity index: measurement techniques and their impact on interpreting cellulase performance. Biotechnol Biofuels 31(3):1–10. https://doi.org/10.1186/1754-6834-3-10

Persson J, Chanzy H, Sugiyama J (1991) Combined infrared and electron diffraction study of the polymorphism of native celluloses. Macromolecules 24:2461–2466. https://doi.org/10.1021/ma00009a050

Phadagi R, Singh S, Hashemi H et al (2021) Understanding the role of dimethylformamide as co-solvents in the dissolution of cellulose in ionic liquids: experimental and theoretical approach. J Mol Liq 328:115392. https://doi.org/10.1016/j.molliq.2021.115392

Poletto M, Zattera AJ (2017) Mechanical and dynamic mechanical properties of polystyrene composites reinforced with cellulose fibers. J Thermoplast Compos Mater 30:1242–1254. https://doi.org/10.1177/0892705715619967

Poletto M, Zattera AJ, Forte MMC, Santana RMC (2012) Thermal decomposition of wood: Influence of wood components and cellulose crystallite size. Bioresour Technol 109:148–153. https://doi.org/10.1016/J.BIORTECH.2011.11.122

Poletto M, Ornaghi Júnior HL, Zattera AJ (2014) Native cellulose: structure, characterization and thermal properties. Materials (basel) 7:6105–6119. https://doi.org/10.3390/ma7096105

Prakash Menon M, Selvakumar R, Suresh Kumar P, Ramakrishna S (2017) Extraction and modification of cellulose nanofibers derived from biomass for environmental application. RSC Adv 7:42750–42773. https://doi.org/10.1039/c7ra06713e

Qasim U, Osman AI, Al-Muhtaseb AH et al (2021) Renewable cellulosic nanocomposites for food packaging to avoid fossil fuel plastic pollution: a review. Environ Chem Lett 19:613–641

Rambabu N, Panthapulakkal S, Sain M, Dalai AK (2016) Production of nanocellulose fibers from pinecone biomass: evaluation and optimization of chemical and mechanical treatment conditions on mechanical properties of nanocellulose films. Ind Crops Prod 83:746–754. https://doi.org/10.1016/j.indcrop.2015.11.083

Sanchez-Salvador JL, Campano C, Lopez-Exposito P et al (2021) Enhanced morphological characterization of cellulose nano/microfibers through image skeleton analysis. Nanomaterials. https://doi.org/10.3390/nano11082077

Scherrer P (1912) Bestimmung der inneren Struktur und der Größe von Kolloidteilchen mittels Röntgenstrahlen. Kolloidchemie Ein Lehrbuch. Springer, Berlin, pp 387–409

Seddiqi H, Oliaei E, Honarkar H et al (2021) Cellulose and its derivatives: towards biomedical applications. Cellul 284(28):1893–1931. https://doi.org/10.1007/S10570-020-03674-W

Segal L, Creely JJ, Martin AE, Conrad CM (1959) An empirical method for estimating the degree of crystallinity of native cellulose using the X-ray diffractometer. Text Res J 29:786–794. https://doi.org/10.1177/004051755902901003

Shaghaleh H, Xu X, Wang S (2018) Current progress in production of biopolymeric materials based on cellulose, cellulose nanofibers, and cellulose derivatives. RSC Adv 8:825–842. https://doi.org/10.1039/c7ra11157f

Shankaran DR (2018) Cellulose nanocrystals for health care applications. Appl Nanomater. https://doi.org/10.1016/B978-0-08-101971-9.00015-6

Sharma S, Nair SS, Zhang Z et al (2015) Characterization of micro fibrillation process of cellulose and mercerized cellulose pulp. RSC Adv 5:63111–63122. https://doi.org/10.1039/c5ra09068g

Sharma A, Thakur M, Bhattacharya M et al (2019) Commercial application of cellulose nano-composites—a review. Biotechnol Rep 21:e00316. https://doi.org/10.1016/j.btre.2019.e00316

Sheng JJ (2011) Polymer flooding. In: Modern chemical enhanced oil recovery. Gulf Professional Publishing, pp 101–206

Šturcova A, His I, Apperley DC et al (2004) Structural details of crystalline cellulose from higher plants. Biomacromol 5:1333–1339. https://doi.org/10.1021/bm034517p

Tarrés Q, Oliver-Ortega H, Boufi S et al (2020) Evaluation of the fibrillation method on lignocellulosic nanofibers production from eucalyptus sawdust: a comparative study between high-pressure homogenization and grinding. Int J Biol Macromol 145:1199–1207. https://doi.org/10.1016/j.ijbiomac.2019.10.046

Trache D, Tarchoun AF, Derradji M et al (2020) Nanocellulose: from fundamentals to advanced applications. Front Chem 8:392

Turbak AF, Snyder FW, Sandberg KR (1983) United States Patent: 4374702

Velásquez-Cock J, Gañán P, Posada P et al (2016) Influence of combined mechanical treatments on the morphology and structure of cellulose nanofibrils: thermal and mechanical properties of the resulting films. Ind Crops Prod 85:1–10. https://doi.org/10.1016/j.indcrop.2016.02.036

Wada M, Okano T, Sugiyama J (2001) Allomorphs of native crystalline cellulose I evaluated by two equatorial d-spacings. J Wood Sci 47:124–128. https://doi.org/10.1007/BF00780560

Wang R, Rosen T, Zhan C et al (2019) Morphology and flow behavior of cellulose nanofibers dispersed in glycols. Macromolecules 52:5499–5509. https://doi.org/10.1021/acs.macromol.9b01036

Wang L, Li K, Copenhaver K et al (2021) Review on non-conventional fibrillation methods of producing cellulose nanofibrils and their applications. Biomacromol 22:4037–4059. https://doi.org/10.1021/ACS.BIOMAC.1C00640/ASSET/IMAGES/ACS.BIOMAC.1C00640.SOCIAL.JPEG_V03

Yuan T, Zeng J, Wang B et al (2021) Cellulosic fiber: mechanical fibrillation-morphology-rheology relationships. Cellulose 28:7651–7662. https://doi.org/10.1007/S10570-021-04034-Y/FIGURES/6

Zimmermann T, Bordeanu N, Strub E (2010) Properties of nanofibrillated cellulose from different raw materials and its reinforcement potential. Carbohydr Polym 79:1086–1093. https://doi.org/10.1016/j.carbpol.2009.10.045

Zuluaga R, Putaux JL, Cruz J et al (2009) Cellulose microfibrils from banana rachis: effect of alkaline treatments on structural and morphological features. Carbohydr Polym 76:51–59. https://doi.org/10.1016/j.carbpol.2008.09.024